Influence of the Axial Ligands on the Spectral Properties of P700 of Photosystem I: A Study of Site-Directed Mutants †

ARTICLE *in* BIOCHEMISTRY · NOVEMBER 2000

Impact Factor: 3.02 · DOI: 10.1021/bi001200q · Source: PubMed

8 AUTHORS, INCLUDING:

Ludwig Krabben
Freie Universität Berlin
13 PUBLICATIONS **386** CITATIONS
SEE PROFILE

Donatella Carbonera
University of Padova
91 PUBLICATIONS **1,521** CITATIONS
SEE PROFILE

Andrew N Webber
Arizona State University
82 PUBLICATIONS **2,173** CITATIONS
SEE PROFILE

Influence of the Axial Ligands on the Spectral Properties of P700 of Photosystem I: A Study of Site-Directed Mutants†

Ludwig Krabben,‡,⊥ Eberhard Schlodder,‡ Rafael Jordan,‡ Donatella Carbonera,§ Giovanni Giacometti,§ Hyeonmoo Lee,|| Andrew N. Webber,|| and Wolfgang Lubitz*,‡

Max-Volmer-Institut für Biophysikalische Chemie und Biochemie, Technische Universität Berlin, Strasse des 17, Juni 135, D-10623 Berlin, Germany, Dipartimento di Chimica Fisica Universita di Padova, Via Loredan 2, 35131 Padova, Italy, and Department of Plant Biology and Center for the Study of Early Events in Photosynthesis, Arizona State University, Tempe, Arizona 85287

Received May 25, 2000; Revised Manuscript Received August 14, 2000

ABSTRACT: Two histidines provide the axial ligands of the two chlorophyll *a* (Chl *a*) molecules which form the primary electron donor (P700) of photosystem I (PSI). Histidine 676 in the protein subunit PsaA, His(A676), and histidine 656 in subunit PsaB, His(B656), were replaced in the green algae *Chlamydomnas reinhardtii* by site-directed mutagenesis with nonpolar, uncharged polar, acidic, and basic amino acid residues. Only the substitutions with uncharged polar residues led to a significant accumulation of PSI in the thylakoid membranes. These PSI complexes were isolated and the physical properties of the primary donor characterized. The midpoint potential of $P700^{+\bullet}$/P700 was increased in all mutants (up to 140 mV) and showed a dependence on size and polarizability of the residues when His(B656) was substituted. In the light-minus-dark absorbance spectra, all mutations in PsaB exhibited an additional bleaching band at 665 nm at room temperature comparable with the published spectrum for the replacement of His(B656) with asparagine [Webber, A. N., Su Hui, Bingham, S. E., Käss, H., Krabben, L., Kuhn, M., Jordan, R., Schlodder, E., and Lubitz, W. (1996) *Biochemistry 35*, 12857−12863]. Substitutions of His(A676) showed an additional shoulder around 680 nm. In the low-temperature absorbance difference spectra of $P700^{+\bullet}$/P700, a blue shift of the main bleaching band by 2 nm and some changes in the spectral features around 660 nm were observed for mutations of His(B656) in PsaB. The analogous substitution in PsaA showed only a shift of the main bleaching band. Similar effects of the mutations were found in the ^{3}P700/P700 absorbance difference spectra at low temperatures ($T = 2$ K). The zero-field splitting parameters of ^{3}P700 were not significantly changed in the mutated PSI complexes. The electron spin density distribution of $P700^{+\bullet}$, determined by ENDOR spectroscopy, was only changed when His(B656) was replaced. In all measurements, two general observations were made. (i) The replacement of His(B656) had a much stronger impact on the physical properties of P700 than the mutation of His(A676). (ii) The exchange of His(B656) with glutamine induces the smallest changes in the spectra or the midpoint potential, whereas the other replacements exhibited a stronger but very similar influence on the spectroscopic features of P700. The data provide convincing evidence that the unpaired electron in the cation radical and the triplet state of P700 are mainly localized on the Chl *a* of the dimer which is axially coordinated by His(B656).

Photosystem I (PSI)[1] is part of the light-driven electron transport chain in the chloroplasts of higher plants and green algae and in photosynthetic cyanobacteria. The PSI complex utilizes light energy to transfer electrons from plastocyanin on the lumenal side of the thylakoid membrane to ferredoxin on the stromal side across a 700 mV energy gap (for reviews, see refs *1*−*3*). The cofactors involved in the charge separation and electron-transfer process are coordinated by the PsaA and PsaB protein subunits, and by PsaC that binds the terminal iron−sulfur clusters, F_A and F_B. PsaA and PsaB are homologous proteins, each consisting of 11 transmembrane α-helices that are more than 80% similar (*4*, *5*).

Electron transfer in PSI is started by the light-induced photooxidation of the primary electron donor P700 with a

† This work was supported by the Deutsche Forschungsgemeinschaft (Sfb 312, TP A4/TP A5, and Sfb 498, TP A1), the National Research Initiatives Competitive Grants Program of the U.S. Department of Agriculture (98-35306-6601), the NATO (CRG950759), European Union TMR Research Network Grant FRX-CT98-0214, and the Deutscher Akademischer Austauschdienst (D/94/14871).

* To whom correspondence should be addressed.

‡ Technische Universität Berlin.

§ Current address: Forschungsinstitut für Molekulare Pharmakologie, Alfred-Kowalke-Strasse 4, 10315 Berlin, Germany.

|| Dipartimento di Chimica Fisica Universita di Padova.

⊥ Arizona State University.

[1] Abbreviations: ADMR, absorption-detected magnetic resonance; *β*-DM, *n*-dodecyl *β*-D-maltoside; BChl, bacteriochlorophyll; (B)Pheo, (bacterio)pheophytine; (b)RC, (bacterial) reaction center; Chl(s) *a*, chlorophyll(s) *a*; ENDOR, electron nuclear double resonance; EPR, electron paramagnetic resonance; hfc(s), hyperfine coupling constant(s); PSI, photosystem I; PSII, photosystem II; T − S, triplet-minus-singlet; WT, wild type.

10.1021/bi001200q CCC: $19.00
Published on Web 09/28/2000

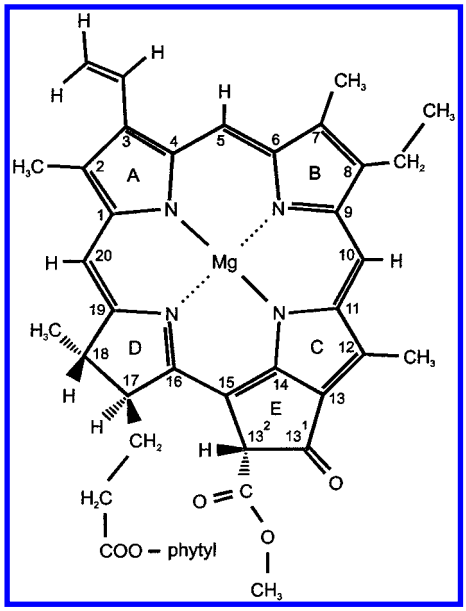

FIGURE 1: Molecular structure and IUPAC numbering scheme for chlorophyll *a* (Chl *a*).

near-unity quantum yield. P700 is a dimer of excitonically coupled chlorophyll *a* (Chl *a*) molecules, P_A and P_B, coordinated by PsaA and PsaB. The structure of Chl *a* is shown in Figure 1. P700 in the lowest excited state donates an electron to the primary acceptor A_0, a Chl *a* monomer. Subsequent charge stabilization is achieved by electron transfer to a series of sequential electron acceptors. Although all types of photosystems [PSII, bacterial reaction centers (bRCs), and RCs from green sulfur bacteria] share a similar cofactor arrangement, they differ strongly in their redox potential. Indeed, the photosystems include the redox protein complexes with the highest oxidation and reduction power known in biological systems, namely, PSII and PSI, respectively. Because of these extraordinary properties, the primary electron donors have been the subject of sustained interest. In bRCs, whose structure has been refined to 2.1 Å resolution (*6*), the dimer consists of two bacteriochlorophylls (BChl) that are axially coordinated by two histidine residues from the protein subunits. The spectroscopic analysis of wild-type bRCs and several mutants in the surroundings of the BChl dimer has revealed that in the oxidized state the positive charge is shared between the two BChls in the ratio of 2:1 (*7*, *8*). The spin distribution and also the redox potential are influenced by modification of the protein environment by site-directed mutagenesis (*9*). Although significant progress has been made in determining the crystal structure of PSI (*10*, *11*) the electronic structure of its cation radical or the localization of the triplet state is still a matter of debate. From ENDOR and ESEEM experiments performed on frozen solutions and single crystals of PSI, an asymmetrical spin distribution ranging from 3:1 to 10:1 was derived (*12*−*15*); even a complete localization on a single Chl *a* was recently proposed (*16*). In contrast, a delocalization of the unpaired electron over both halves of the dimer with a ratio of 1:1 to 2:1 and a localization of the triplet state on one Chl *a* were suggested from a recent analysis of P700, $P700^{+\bullet}$, and $^3P700$ using vibrational spectroscopy (*17*).

In this work, we address the question how the axial ligands of the dimer affect the physical properties of the primary donor in PSI. From sequence comparisons and earlier mutagenesis studies, the histidines His(A676) in subunit PsaA and His(B656) in subunit PsaB were believed to provide the axial coordination of P700 (*18*−*21*). These histidines are located in the transmembrane spans X, which are named helix m and m′ in the crystal structure (*10*, *11*), Very recently, the refinement of the crystal structure of PSI from *Synechococcus elongatus* at 2.5 Å resolution confirmed that these histidines are close to the two Chl *a* molecules forming P700 (called eC_1 and eC_1' in the 4 Å structural model) and point toward the Mg atoms (P. Jordan, P. Fromme, O. Klukas, W. Saenger, H. T. Witt, and N. Krauss, personal communication). We have replaced histidine 676 in the PsaA protein subunit [His(A676)] and histidine 656 in the PsaB subunit [His(B656)] of the green algae *Chlamydomonas reinhardtii* with nonpolar, uncharged polar, acidic, and basic amino acid residues. In the analyzed mutants, only the substitutions with uncharged polar residues led to a significant accumulation of PSI in the thylakoid membranes. The modified PSI particles were isolated, and the influence of the amino acid replacements on the following physical properties of the primary electron donor was probed: (i) the oxidation midpoint potential, (ii) the optical characteristics of P700, (iii) the parameters of its triplet state, and (iv) the spin density distribution of $P700^{+\bullet}$. For this endeavor, redox titrations, optical spectroscopy as well as ADMR, EPR, and ENDOR techniques have been employed (*22*). The influence of the introduced amino acid side chain and the distinct differences between homologous mutations in PsaA and PsaB on P700 will be discussed. The results show that in the oxidized $P700^{+\bullet}$, the unpaired electron is mainly localized on that half of the dimer which is coordinated by subunit PsaB.

MATERIALS AND METHODS

Site-Directed Mutagenesis and Chloroplast Transformation of C. reinhardtii. Oligonucleotide-mediated site-directed mutagenesis was used to introduce mutations into the *psaA* and *psaB* genes. For *psaB*, the protocol has already been described (*18*). For mutations in *psaA*, an *Avr*II−*Bam*HI fragment from chloroplast DNA restriction enzyme fragment *Bam* 11, containing a portion of *psaA* exon 3, was used as a template for mutagenesis (*23*). The *aadA* gene was then blunt-end ligated into an *Eco*RI restriction enzyme site located downstream of *psaA* exon 3 (*23*) to give the final construct used for chloroplast transformation. Particle bombardment of *C. reinhardtii* cells and antibiotic selection of chloroplast transformants were performed as previously described (*18*, *23*).

Strains and Media. Strain CC2696 of *C. reinhardtii* was used as the recipient of donor plasmids in the transformation experiments as described in refs *24* and *25*. This mutant strain carries the DS521 cab deficiency mutation and *psbA* deletion mutation (*26*). Comparison of the PSI complexes isolated from strain CC2696 with PSI preparation from FUD7 or CC125 strains showed no significant difference in the experiments described in this work. We, therefore, refer to these preparations without mutation as WT. Site-directed mutants in which His-676 of subunit PsaA is replaced with Ser are called HS(A676) and analogous for the mutants in subunit PsaB [HS(B656)] following the nomenclature in ref *20*. Cells were grown in Tris-acetate-phosphate medium

(TAP) and high-salt medium containing acetate according to the method described in ref *27*. If necessary, the media were solidified with 2% bacto agar (Difco) and supplemented with spectinomycin. Algae were grown heterotrophically at 27 °C in 15 L carboys under low-light conditions (≤ 1 μE m^{-2} s^{-1}).

Preparation of PSI Complexes from the CC2696 Strain. Because of the different background strain CC2696, we have modified the preparation of PSI complexes as follows. Cells from 30 L of medium were harvested during exponential growth at a density of 2×10^6 cells/mL with a continuous flow centrifuge (CEPA) and washed two times with 50 mM Tricine (pH 7.5) and 10 mM EDTA and resuspended in the same buffer at a density of 2×10^8 cells/mL. Cells were broken using three rounds of sonification (1 min and 30 s at power level 8 and with a pulse duration of 50% with a 3 min break) using a Branson 450 Sonifier. The homogenate was centrifugated at 200000*g* for 25 min, and the crude thylakoids were washed in 0.5 M NaCl and 20 mM Tricine (pH 7.5), collected at 50000*g* for 20 min, washed, and resuspended in 50 mM Tricine (pH 7.5). Crude thylakoids were frozen in liquid nitrogen and stored at −80 °C until further preparation could be carried out. To obtain PSI particles, thylakoids corresponding to 70 g of wet cell weight were solubilized at 4 °C for 90 min in 180 mL of 50 mM Tricine (pH 7.5) containing 1% *n*-dodecyl β-D-maltoside (β-DM) and protease inhibitor cocktail (Complete from Boehringer Mannheim). The solubilized thylakoids were centrifuged at 50000*g* for 20 min. The supernatant (25 mL) was loaded on a 5 mL 40% sucrose cushion and centrifuged at 360000*g* for 90 min. The green band on top of the sucrose cushion was collected and loaded onto a size exclusion column 130 cm in length and 2.5 cm in diameter (Sepharose CL6B/Pharmacia) equilibrated in 20 mM MES (pH 6.5), 1 mM EDTA, and 0.02% β-DM. At a flow rate of 1 mL/min, the PSI-containing fractions eluted after approximately 6 h in a peak fraction before the light-harvesting complexes eluted. The PSI fractions were pooled and concentrated in ultrafiltration devices with a 100 000 kDa molecular mass cutoff (Ultrafree/Millipore).

Optical Spectroscopy. The flash-induced absorbance spectra at room temperature were recorded using a laboratory-built flash spectrometer (*28*). The measuring light from a 55 W tungsten halogen lamp was passed through a monochromator with a spectral bandwidth of 3 nm, an optical cuvette 1 cm in length, and a combination of interference and edge filters in front of a photomultiplier (EMI 9558BQ) coupled to a transient recorder (Tektronix TDS320). The samples were excited by saturating Xe flashes about 15 μs in length filtered by colored glass (CS96-4 from Corning). Before the measurements, the PSI complexes were diluted to 10 μM Chl in 20 mM Tricine (pH 7.5), 5 mM $MgCl_2$, 0.02% β-DM, 5 mM sodium ascorbate, and 5 μM phenazine methosulfate. The time course of the absorbance changes was fitted to an exponential decay using an algorithm that minimizes the sum of the unweighted least squares. The concentration of P700 was calculated from the maximal absorbance decrease in the Q_y-region. The difference in the extinction coefficients between P700 and $P700^{+\bullet}$ at the peak wavelength was determined from the flash-induced absorption change of *N*,*N*,*N*,*N*-tetramethyl-*p*-phenylenediamin dihydrochlorid (TMPD) according to the method described in ref *29*. The TMPD is oxidized by the flash-induced $P700^{+\bullet}$. A value of 110 mM^{-1} cm^{-1} was obtained for WT PSI complexes at 696 nm.

The light-minus-dark spectra at 77 K were measured using a liquid nitrogen bath cryostat (DN 1704 from Oxford). PSI complexes were diluted to 10 μM Chl in 60% glycerol, 20 mM Tricine (pH 7.5), 5 mM $MgCl_2$, and 5 mM sodium ascorbate. Two milliliters of the sample was brought into the cryostat under an argon stream at room temperature and dark adapted for at least 30 min. The cryostat was cooled to liquid nitrogen temperature and centered in the measuring beam of a CARY 5 spectrophotometer (Varian) using a home-built cryostat holder. The dark spectrum was recorded from 600 to 750 nm at 0.1 nm data intervals (20 nm/min) with a spectral bandwidth of 1 nm. After 10 saturating Xe flashes, the light spectrum was recorded in the same way. The light-minus-dark difference spectra reflect absorbance changes due to the oxidation of P700.

Redox Titration. The oxidation midpoint potential (E_m) of P700 was determined at room temperature by measuring the magnitude of the flash-induced absorbance increase at 826 nm, associated with oxidation of P700, as a function of the redox potential. For titrations, PSI complexes were diluted to 20−30 μM Chl in 20 mM Tricine (pH 7.5), 100 mM KCl, 5 mM $MgCl_2$, and 0.02% β-DM. The redox potentials were adjusted with mixtures of ferricyanide and ferrocyanide up to a total concentration of 8 mM. After each experiment, the potential was measured using a combination Pt/Ag/AgCl electrode (Schott PT5900A) which was calibrated against the redox potential of a saturated solution of quinhydrone as a function of pH. A Knick pH-meter (PHM82) was used to read out the redox potential. All redox potentials are given relative to the standard hydrogen electrode (NHE).

EPR and ENDOR Spectroscopy. An X-band EPR spectrometer (Bruker ESP 300E) was used equipped with a helium cryostat (Oxford A 910) and a standard rectangular cavity (Bruker ER 4102 ST). The microwave frequency was measured with a Hewlett-Packard 532B microwave counter and the magnetic field with a Bruker ER035 NMR-Teslameter. To measure $P700^{+\bullet}$ activity in the mutants, cells from a fresh culture were collected and washed three times with 50 mM Tricine and 5 mM $MgCl_2$. The cells were incubated with 10 mM ferricyanide to chemically oxidize P700 or with 10 mM sodium ascorbate in the dark for 20 min to keep PSI in the reduced state. The suspensions were introduced into 4 mm outer diameter EPR tubes (Wilmad 707SQ), and cells were pelleted at 1000*g* in these tubes. The supernatant was discarded, and the samples were frozen in liquid nitrogen. It was ensured that the cells were in the same growth phase and that the volume in the EPR tube covered more than the active area of the resonator. The samples containing sodium ascorbate were first measured in the dark. After illumination at room temperature and freezing, the light-induced signal was measured. The EPR signals were recorded under identical experimental conditions: nonsaturating microwave power of 26 μW, field modulation frequency of 100 kHz, field modulation depth of 0.1 mT, conversion time of 42 s, 20 scans, and $T = 20$ K. The detection limit of $P700^{+\bullet}$ in cells under our experimental conditions was $3 \pm 1\%$ with respect to the WT intensity with an error of 30% for each measurement.

ENDOR measurements were performed on a Bruker ESP 300E X-band EPR spectrometer with home-built ENDOR accessories (*30*). A TM_{110}-type microwave cavity (radio frequency coil arrangement similar to that in ref *31*) was used which provided a good *Q* factor, resulting in high ENDOR sensitivity. The sample temperature was controlled using a Bruker ER4111 VT nitrogen flow system. ENDOR experiments were performed on the cation radical $P700^{+\bullet}$ of PSI complexes in frozen solution at 160 K as described previously (*18*, *20*). Measurements were carried out at a chlorophyll concentration of 5 mM for WT and 1−4 mM for mutants depending on the yield of PSI. P700 was generated by continuous illumination for 1 min at room temperature with a 1000 W tungsten lamp equipped with a water filter (8 cm path length) and heat absorbing filter glasses followed by rapid freezing.

ZF-ADMR and ODMR Spectroscopy of the P700 Triplet State. PSI particles were diluted to final concentrations ranging from 50 to 100 μM Chl in 50 mM Tricine (pH 7.5), 5 mM $MgCl_2$, and 0.02% β-DM. Oxygen was removed using a glucose/glucose oxidase system (*32*). Dithionite (20 mM) was added to this solution under nitrogen. Glycerol was added to a final concentration of 60% to all the samples to obtain a transparent glass. Before being frozen in the cryostat, the samples were illuminated for a period of 5 min at room temperature under ventilation with strong white light from a 1000 W focused tungsten lamp filtered by water (10 cm path length) and additional heat absorbing filters. Via this treatment, reduction of the secondary electron acceptor, the phylloquinone A_1, was achieved. When the electron transfer to A_1 is blocked, the primary radical pair, $P700^{+\bullet}A_0^{-\bullet}$, recombines with high yield to the triplet state of P700 as reported previously (*33*). In a previous publication (*34*), the same procedure was shown to induce P700 triplet formation that could be detected by ODMR spectroscopy in thylakoids and PSI-200 particles (containing 200 chlorophyll molecules per PSI) of higher plants. All the measurements were performed at 1.7 K. The absorption-detected magnetic resonance (ADMR) and the triplet-minus-singlet (T − S) microwave-induced spectra were recorded using the laboratory-built apparatus described in ref *35*.

RESULTS

Site-Directed Mutagenesis and Characterization of the Mutant Phenotypes. All mutations except HD(B656) and HR(B656) were introduced in the CC2696 background strain (*36*). The phenotype of this strain has a decreased abundance of light-harvesting complexes (10%) and is PSII deficient (*26*). PSI is therefore the main chlorophyll binding protein in this strain. An inspection of the phenotype by eye already indicated that the amount of PSI was reduced in the mutated cells. The replacement of His with Leu and Phe resulted in a yellowish phenotype irrespective of the modified subunit (PsaA or PsaB) that was chosen, indicating a very low level of or no stable accumulation of PSI. The replacement by Cys in PsaA showed the same phenotype. Mutants HS(A676), HS(B656), HN(B656), HG(B656), and HC(B656) accumulated PSI to a moderate level, giving rise to a green-yellowish color in the cultures. Mutants containing Gln exhibit no observable difference with respect to the CC2696 background strain. A change in the phenotype of HD(B656) and HR(B656) could not be observed as the background strain FUD7 contained normal amounts of light-harvesting complexes.

Isolation of PSI from the Mutants. Almost all the methods described in the literature for isolation of PSI use the solubilization of the thylakoid membranes with detergent and a separation of the chlorophyll binding complexes after centrifugation on a linear sucrose gradient, first reported in ref *37*. For mutants containing small amounts of PSI, this method showed a poor or no separation of PSI from the light-harvesting complexes (*38*). The yield and the purity of such preparations were not sufficient for the characterization of the mutants. To circumvent this problem, strain CC2696 of *C. reinhardtii*, which has a small amount of light-harvesting complexes and lacks the PSII complex (*26*), was used together with a modified preparation method to isolate PSI from the mutants. After solubilization of the thylakoid membranes, size exclusion chromatography led to the rapid isolation of the PSI. This ensured a high yield and sufficient purity of the PSI complexes. However, the described method is not recommended for strains containing normal amounts of light-harvesting complexes, since in this case a sufficient separation by size exclusion chromatography is not possible. The PSI-containing fraction had a ratio of 80−120 Chls per PSI for WT preparations. The yield of PSI complexes from the mutants HS(A676), HS(B656), HN(B656), HG(B656), and HC(B656) was approximately 50% of the WT amount. Due to the smaller overall level of PSI, contamination by light-harvesting protein complexes becomes more severe. Therefore, the Chl to PSI ratios increased up to 300. In the preparations from HL(A676), HC(A676), HL(B656), and HF(B656), no formation of $P700^{+\bullet}$ was detected by means of flash-induced absorbance difference spectroscopy, neither in thylakoids nor in the fractions after size exclusion chromatography. The yield of PSI for HF(A676) was also not sufficient for further characterization.

EPR Spectroscopy of $P700^{+\bullet}$ Generated in Whole Cells. To investigate whether PSI is present in the preparation, and whether the P700 cation radical is formed in the cells, we measured the EPR signal of $P700^{+\bullet}$ in whole cells of WT and mutants. Although EPR is a very sensitive method for detecting radicals, an accurate quantitative determination is difficult. To ensure identical experimental conditions, the volume of cells in the EPR tubes fully covered the resonant area of the cavity. The intensity of the EPR signal was obtained by double integration of the first-derivative EPR spectrum. Since the EPR signal depends on several parameters, which vary slightly from sample to sample, the intensity can only be used as a rough estimate of the PSI abundance in the cells. Several measurements with different WT cell preparations showed that the intensity of the EPR signal was reproducible within an error of about 30%. For each mutant, the stable radical was generated in two ways: (i) chemical oxidation with ferricyanide to ensure the oxidation of P700 even in the case where the mutation might block the light-driven electron transfer and (ii) trapping the $P700^{+\bullet}$ state by freezing the sample under saturating illumination. As control for background signals near $g = 2.00$, the latter sample containing ascorbate was measured prior to illumination. In no case was a significant signal detected in these dark-adapted samples.

Table 1: PSI Abundance in the Thylakoid Membranes or Whole Cells of PSI Mutants of *C. reinhardtii* Compared with the WT Abundance

type of side chain	PsaA		PsaB	
nonpolar	HL(A676)	−[a]	HL(B656)	+
	HF(A676)	10−30[b]	HF(B656)	−
uncharged polar	HQ(A676)	60−100	HQ(B656)	60−100
	HS(A676)	40−70	HS(B656)	40−70
	HC(A676)	+[c]	HC(B656)	40−70
			HG(B656)	40−70
			HN(B656)	40−70
acidic			HD(B656)	+
basic			HR(B656)	−

[a] No PSI activity with either method. [b] The amount of PSI (in % relative to WT) was estimated from flash-induced absorbance changes ΔA of thylakoids and EPR signal intensities of whole cells after incubation with ferricyanide as described in the Results. For the measurement of ΔA, the cells were broken and thylakoids were prepared; in addition, β-DM was added to prevent aggregation. [c] $P700^{+\bullet}$ formation was only detected by EPR in cells.

For WT cells, unresolved Gaussian EPR lines of 0.76 ± 0.02 mT (fwhm) were obtained at $g = 2.0026 \pm 0.0001$ ($T = 20$ K), consistent with the values reported for the $P700^{+\bullet}$ cation radical (*39*). The intensity of the EPR signal for samples containing ferricyanide was in all cases higher than the intensity for illuminated samples, indicating incomplete photooxidation of P700. However, both methods lead to the same results, when the intensities of the EPR signals of the mutants were normalized with respect to that of the WT. The EPR data are in good agreement with the observed phenotypes of the mutants and the measurements of the PSI amount by optical flash-induced absorbance difference spectroscopy using thylakoid membranes. Table 1 shows the amounts of PSI for the mutations in PsaA and PsaB relative to that in WT. Substitution of the histidines with acidic, basic, or nonpolar amino acid residues leads to a drastic decrease in the magnitude of the $P700^{+\bullet}$ signal. The replacement with uncharged polar amino acid residues exhibits moderate accumulation of PSI. In the case of HC(A676), oxidation of P700 was only observed by EPR spectroscopy in whole cells, and was not detected by absorption difference spectroscopy using thylakoids.

Oxidation Midpoint Potential of $P700^{+\bullet}$/P700. The midpoint potential of $P700^{+\bullet}$/P700 is surprisingly small compared with that of Chl *a* in organic solvents, which is at least 200 mV more positive (*40*). It is not clear to what extent the structural organization of the two Chl *a* molecules or their protein environment is responsible for this strong decrease. This essential functional property of the redox couple $P700^{+\bullet}$/P700 is therefore assumed to be a characteristic and sensitive probe for changes of the environment of the primary donor. Figure 2 shows the redox titration curves for all mutants studied in this study and in our previous work (*19*, *20*). The data were fitted using the one-electron Nernst equation ($n = 1$).

In all mutants, the midpoint potential is increased compared with the value of WT (447 ± 6 mV). An increase of about 20 mV was obtained for mutations HQ(A676) and HS(A676). About the same increase was measured for mutation HQ(B656). The 40 mV increase for HN(B656) and HS(B656) was previously reported (*19*, *20*) for PSI from FUD7 but was confirmed for preparations from *C. reinhardtii* strain CC2696 used in this work. The replacement of His-B656 with Gly and Cys, respectively, increased the midpoint potential by 100 and 140 mV, respectively.

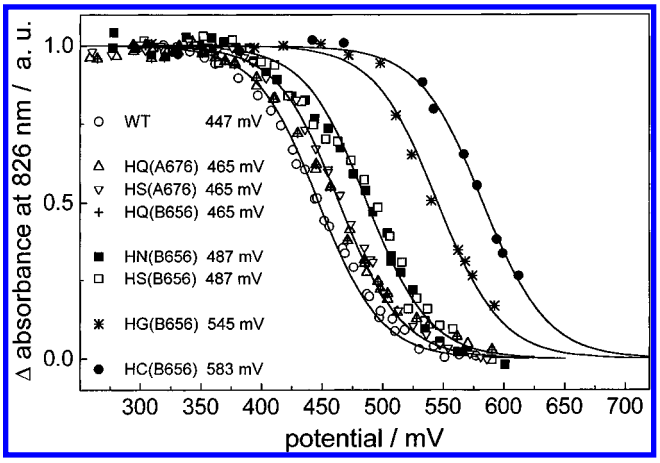

FIGURE 2: Redox titration of the flash-induced absorption change at 826 nm in PSI complexes of *C. reinhardtii*. The absorbance increase at 826 nm is attributed to formation of $P700^{+\bullet}$: WT (○), $E_m = 447$ mV; HQ(A676) (△), HS(A676) (▽), and HQ(B656) (+), $E_m = 465$ mV; HN(B656) (■) and HS(B656) (□), $E_m = 487$ mV; HG(B656) (∗), $E_m = 545$ mV; and HC(B656) (●), $E_m = 583$ mV. The error is ±6 mV for all measurements. Solid lines represent the best fits to the data using the one-electron Nernst equation ($n = 1$). The data for HN(B656) and HS(B656) were taken from ref *20*.

Optical Spectroscopy at Room Temperature and 77 K. The optical features of the primary electron donor were studied using absorbance difference spectroscopy. The spectra that were obtained represent the absorbance changes due to the oxidation of P700 as a function of wavelength. The flash-induced absorbance difference spectra recorded at room temperature were normalized to the same area under the curve between 650 and 720 nm (Q_y-region). Thereby, we assume that the loss of oscillator strength upon photooxidation of P700 is not significantly altered by the mutation. Direct measurements of the difference of the extinction coefficients between P700 and $P700^{+\bullet}$ at the peak wavelength of the main bleaching band in WT and three mutants confirmed this assumption (not shown).

In Figure 3, the spectra of mutants HQ(A676), HS(A676), HQ(B656), and HS(B656) are compared to that of WT. For reasons of clarity, the spectra of HN(B656), HC(B656), and HG(B656) are omitted; they are virtually identical to the spectrum of HS(B656). The main bleaching band centered at 696 nm in WT dominates the spectra. The PsaA mutants, HQ(A676) and HS(A676), exhibit an additional bleaching band around 680 nm and decreases in the amplitude of the main bleaching band at 696 nm of 13 and 27%, respectively (Figure 3a). Mutations HS(B656) (see Figure 3b) and HG(B656) as well as HC(B656) (not shown) exhibit an additional bleaching band around 665 nm. The same feature has previously been reported for HN(B656) (*19*, *20*). In the case of HQ(B656), a broad absorbance decrease is observed between 680 and 655 nm (Figure 3b). For all mutations, the additional bleaching corresponds to a decrease in the amplitude of the main bleaching band by approximately 20%.

To measure the $P700^{+\bullet}$-minus-P700 absorbance difference at low temperature (77 K), the samples were frozen in the presence of 5 mM sodium ascorbate in the dark. At a temperature below 100 K, a stable charge separation

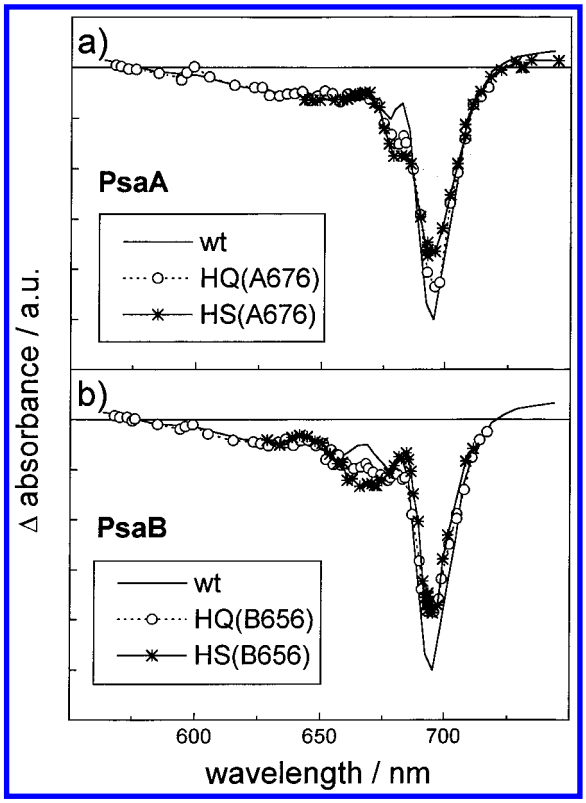

FIGURE 3: Flash-induced absorbance difference spectra of $P700^{+\bullet}$/P700 measured at room temperature. The solid line without symbols (−) represents the spectrum of the wild type (wt), and the lines with symbols represent the spectra of the mutated PSI complexes as indicated in the insets. The samples were excited by saturating flashes about 15 μs in length from a Xe flash lamp. The spectra are normalized to the same bleached area between 650 and 720 nm.

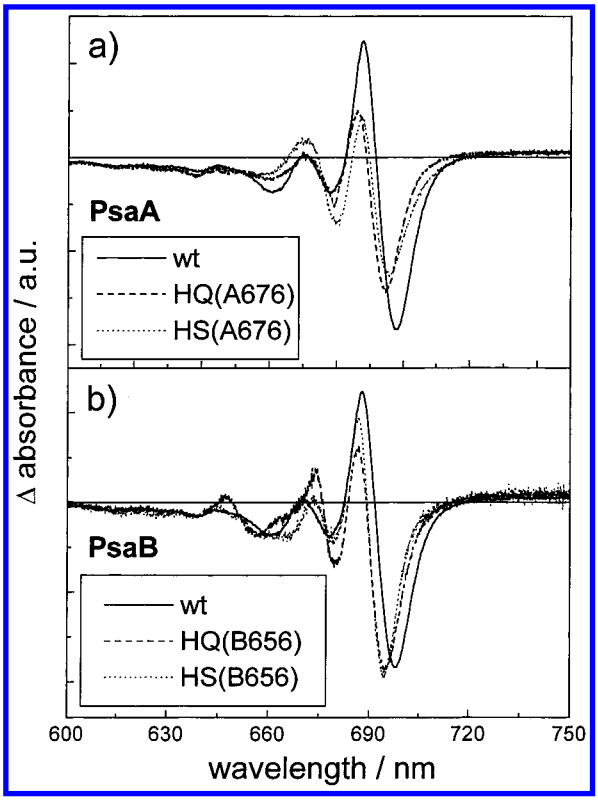

FIGURE 4: Light-minus-dark difference spectra of PSI complexes prepared from *C. reinhardtii* at 77 K. The curves were obtained by subtraction of the absorbance spectra in the dark-adapted state of PSI from the spectra after illumination. The spectra are normalized to the same bleached area between 650 and 720 nm: (a) mutations in PsaA and (b) mutations in PsaB.

($P700^{+\bullet}F_{A/B}^{-\bullet}$) is induced in 80% of the PSI complexes by actinic light. Therefore, the oxidized-minus-reduced spectrum of P700 was obtained by subtraction of the absorbance spectrum at 77 K before illumination from that after 20 Xe flashes. The spectra are normalized to the same area between 650 and 720 nm for the same reasons as described above. The main features of the $P700^{+\bullet}$-minus-P700 absorbance difference spectrum at low temperatures observed with PSI complexes from WT (Figure 4, solid line) are the strong bleaching at 696 nm and a strong absorbance increase at 687 nm. Additionally, the spectrum exhibits smaller absorbance differences at 678 (−), 672 (+), and 666 nm (−). For all mutants, the main bleaching band is shifted to the blue by approximately 2 ± 0.5 nm and the width at half-minimum is decreased with respect to that of WT. For mutants HS and HQ in PsaA, the magnitude of the strong bleaching at 694 nm and the absorbance increase at 687 nm are smaller than in WT (Figure 4a). Mutations in PsaB induce, in addition to the blue shift of the main bleaching band, effects on the spectral features between 650 and 680 nm (Figure 4b). Mutants HG(B656), HC(B656), and HN(B656) in PsaB exhibit spectra virtually identical to that of HS(B656).

Absorbance-Detected Magnetic Resonance in the Absence of an External Magnetic Field (ZF-ADMR). From the zero-field splitting (ZFS) parameters $|D|$ and $|E|$ of the triplet state ^{3}P700 and the T − S spectrum, information can be obtained about the localization of the triplet state in the Chl *a* dimer. In addition, the T − S spectrum contains information about the excitonic interactions of P700 with nearby pigments (*41*). Modification of the geometry of the triplet carrying molecule(s) influences in particular the ZFS parameters which are a measure of the distribution of the triplet state. $|D|$ and $|E|$ are determined from the absorbance change at the resonant microwave frequency at the maximum of the main bleaching band, which varies slightly for the mutants.

The $|D|$ and $|E|$ values obtained from the ADMR measurements are summarized in Table 2. The values for $|D|$ are identical or only slightly increased (1%) in all mutants compared with that of WT. $|E|$ is increased for the mutations in PsaA and for HQ(B656) by about 5.0% and decreased by 2.5% for HS(B656), 5% for HN(B656) and HG(B656), and 7.5% for HC(B656).

Microwave-Induced Triplet-Minus-Singlet (T − S) Difference Spectra of P700. The absorbance difference spectrum, obtained by amplitude modulation (33 Hz) of the microwaves at a fixed resonant frequency corresponding to the $|D| + |E|$ or $|D| - |E|$ transitions of ^{3}P700, reflects the absorbance difference between P700 in its triplet state and in its singlet ground state at 2 K. In the Q_y-region, the T − S spectrum of P700 from *C. reinhardtii* WT PSI preparations is characterized by a strong bleaching at 694.5 nm, a positive peak at 685 nm, a weak absorbance decrease around 680 nm, and an absorbance increase at 671 nm (Figure 5, solid line). The T − S spectra of P700 in the HQ mutants exhibit the smallest differences to the WT spectra (Figure 5, dashed line). In the other mutants, the position of the main bleaching band is shifted to the blue and the width at half-minimum is

Table 2: Comparison of the T − S Spectral Features and ZFS Parameters of the P700 Triplet State from WT and Mutants

	features of the main bleaching band[a]		absorbance changes in the 650−680 nm region[a]		ZFS parameters[c]	
	position	fwhm[b]	increase	decrease	$\|D\|$	$\|E\|$
WT	694.5	9.0	671.0	679	0.0280	0.00395
HQ(A676)	694.5	9.0	671.0	679	0.0280	0.00410
HS(A676)	693.0	8.0	671.0	679	0.0283	0.00415
HQ(B656)	694.0	8.5	671.0	678	0.0280	0.00415
HS(B656)	694.0	7.5	663.5	676	0.0281	0.00385
HC(B656)	693.0	7.0	662.0	672	0.0282	0.00365
HG(B656)	693.0	7.0	661.5	675	0.0281	0.00375
HN(B656)	692.0	6.5	664.0	674	0.0282	0.00375

[a] Values for the absorption bands are in nanometers. [b] The fwhm is the full width measured at half-maximum of the main bleaching band in nanometers. Errors are ±0.5 nm for the main bleaching band and the local absorbance increase around 670 nm and ±2 nm for the local absorbance decrease around 679 nm. [c] ZFS parameters are in inverse centimeters. The errors for $|D|$ and $|E|$ from ADMR measurements are ±0.0001 and ±0.00005 cm^{-1}, respectively.

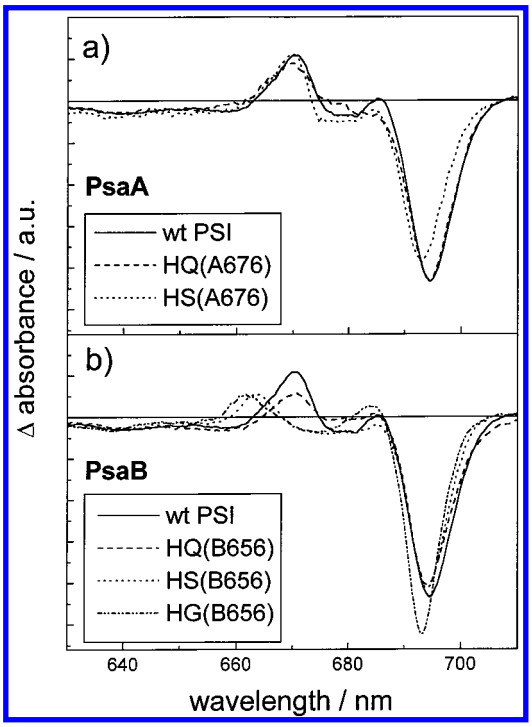

FIGURE 5: T − S spectra of PSI complexes reduced with dithionite and preilluminated at room temperature for 5 min. Data are taken at the maximum of the $|D| + |E|$ transition according to the ZFS values given in Table 3. Experimental conditions were as follows: 1.8 K, 33 Hz modulation frequency, 20 mW microwave power, and 0.1 nm scan rate. Spectra are normalized to the same bleached area between 620 and 720 nm: (a) mutations in PsaA and (b) mutations in PsaB.

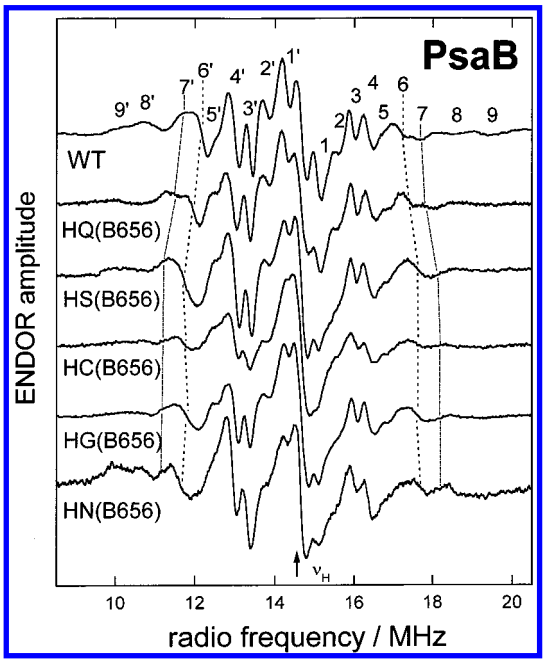

FIGURE 6: ^{1}H ENDOR (electron nuclear double resonance) spectra of $P700^{+\bullet}$ in PSI from *C. reinhardtii* wild type (wt) and PsaB mutants in frozen solution. The prominent principal components of the hfc tensor for the protons of the methyl group at position 12 of the chlorin ring are marked in WT and mutants (*39*): (−•−) $A_{||}$ component (line pair 7′, 7) and (•••) $A_{\perp}$ component (line pair 6′, 6). The spectra for HN(B656) and HS(B656) were taken from ref *20*.

reduced (Table 2). The spectral features on the short-wavelength side of the strong bleaching band are significantly altered upon mutation in PsaB but not in PsaA. The wavelength of the absorbance increase shifts from 670 nm in WT to about 664 nm in HS(B656) and HN(B656) and to 662 nm in HC(B656) and HG(B656) (see Figure 5 and Table 2).

Electron Nuclear Double Resonance Spectroscopy of P700$^{+\bullet}$. The oxidized primary donor $P700^{+\bullet}$ in PSI isolated from WT and mutants has been characterized by EPR and ENDOR spectroscopy in frozen solution at 160 K. The latter method allows the detection of the electron nuclear hyperfine coupling constant (*43*). For all preparations, an unresolved Gaussian EPR line was obtained at $g = 2.0026$ (not shown), indicating no major changes in the electronic structure of $P700^{+\bullet}$. The individual proton hfcs were resolved by ^{1}H ENDOR spectroscopy. Figure 6 compares the powder-type ENDOR spectra obtained for $P700^{+\bullet}$ in WT and the mutants in PsaB. The spectra for HN(B656) and HS(B656) are taken from our previous work (*20*). The largest hfcs (line pairs 9′, 9 and 8′, 8) in the spectrum have been assigned previously (*39*, *44*) to the β-protons of the spin-carrying Chl *a* (position 17; position 18 according to the IUPAC numbering of a Chl *a* which is shown in Figure 1). They were not further evaluated because of the strong line broadening which is difficult to simulate, although some changes in these lines were found for mutations in PsaB. On the basis of the analysis of ENDOR spectra of $P700^{+\bullet}$ obtained in PSI single crystals, the second largest splittings (line pairs 6′, 6 and 7′, 7) belong to the perpendicular and parallel hyperfine tensor components of the CH_3 protons at position 12^1 of the

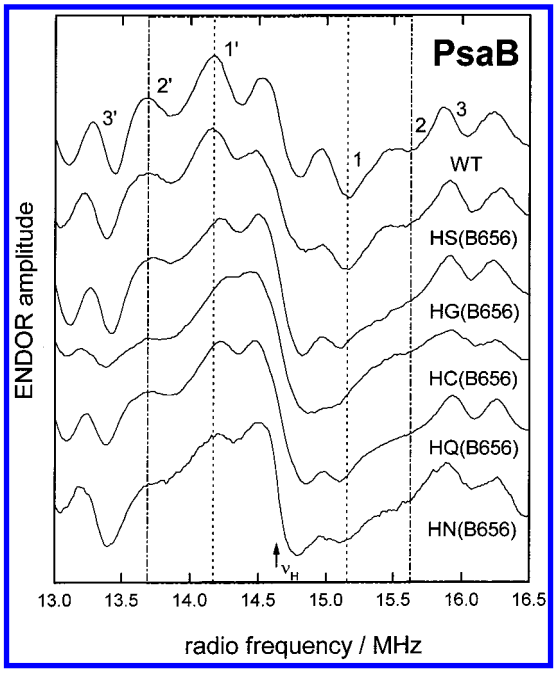

FIGURE 7: Matrix region of the ^{1}H ENDOR spectra for P700$^{+\bullet}$ in PSI of PsaB mutants (Figure 6) between 13 and 16.5 MHz. Two of the prominent line pairs are marked by dotted and dashed lines.

chlorin ring (see Figure 1) (*39*, *44*). Further nested lines (3′, 3 to 5′, 5) were assigned to two other axially symmetric ^{1}H hfc tensors (positions 2 and 7 in Figure 6) of the spin-carrying Chl *a* of P700$^{+\bullet}$. The remaining small hfcs have not yet been assigned with confidence (*39*, *44*).

All mutants in PsaB show an increase in the hfc for the methyl group at position 12 (Figure 6) similar to that reported previously for HN(B656) and HS(B656) (*20*). For the two other methyl group tensors of the spin-carrying Chl *a*, only minor changes in the hfcs were observed which lie within the experimental error limits.

The interpretation of the ENDOR spectrum of the P700 cation radical in single crystals of PSI attributes the electron spin to more than 85% to one of the two Chl *a* molecules comprising the dimer (*39*). In this work, no conclusive proof has, however, been found for the delocalization of spin density onto a second Chl *a* half of a P700 dimer. If there were any spin on a second Chl *a*, the corresponding hfcs would have to be small. The so far unassigned line pairs 1′, 1 and 2′, 2 might contain contributions of these hfcs in addition to hfcs of protons with smaller couplings of the spin-carrying Chl *a* (*39*, *44*). Consequently, we have more thoroughly examined possible changes caused by the mutations in this spectral range (Figure 7). Only slight differences were found for the line shapes of 1′, 1 and 2′, 2 for mutations in PsaB, but the position of the maxima and minima and the turning points remained unaffected within experimental uncertainty. The ENDOR spectra of P700$^{+\bullet}$ of PsaA mutants, HS(A676) and HQ(A676), are all unchanged compared with that of WT (Figure 8). The parallel ($A_{||}$) and perpendicular ($A_\perp$) components of the ^{1}H hfcs of the assigned methyl tensors are summarized in Table 3.

DISCUSSION

In this work, a series of site-directed PSI mutants was studied in which histidines of the two largest subunits of PSI, PsaA and PsaB (His-676 of PsaA and His-656 of PsaB), were replaced with several amino acids (Gly, Ser, Cys, Asn, Gln, Leu, Phe, Asp, and Arg). These histidines are believed to provide the axial ligands to the two Chl *a* molecules, comprising P700 (*18*−*21*). Indeed, the latest refinement of the crystal structure of PSI of *S. elongatus* confirmed that the homologous histidines are pointing to the Mg atoms of the two Chl *a* molecules constituting the dimer (P. Jordan, P. Fromme, O. Klukas, W. Saenger, H. T. Witt, and N. Krauss, personal communication).

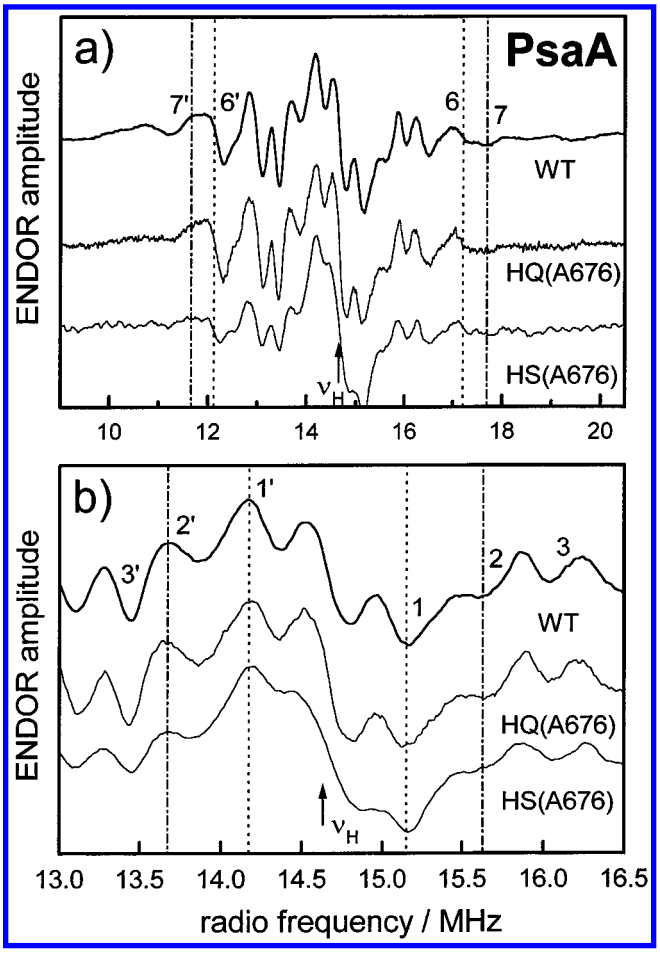

FIGURE 8: ^{1}H ENDOR spectra of P700$^{+\bullet}$ from the wild type and PsaA mutants in frozen solution: (a) full spectral range between 9.0 and 20.5 MHz and (b) enlargement of the matrix region between 13 and 16.5 MHz. Dotted and dashed lines are added to emphasize the unchanged line positions.

Table 3: $A_{||}$ and $A_\perp$ Components of the Methyl Protons Hyperfine Couplings in Megahertz of P700$^{+\bullet}$ from WT and Mutants of *C. reinhardtii*[a]

		$A_{||}(12^b)$	$A_\perp(12)$	$A_{||}(7^b)$	$A_\perp(7)$	$A_{||}(2^b)$	$A_\perp(2)$
WT	His	5.90	5.00	4.30	3.30	3.70	2.60
PsaA	HQ(A676)	6.10	4.90	4.00	3.15	3.75	2.55
	HS(A676)	6.10	5.00	4.30	3.30	3.70	2.60
PsaB	HQ(B656)	6.40	5.25	4.50	3.30	3.75	2.65
	HS(B656)	6.75	5.75	4.30	3.27	3.60	2.65
	HC(B656)	6.65	5.65	4.20	3.25	3.60	2.65
	HG(B656)	6.80	5.60	4.32	3.25	3.90	2.65
	HN(B656)	6.95	6.00	4.55	3.40	3.90	2.70

[a] The error in the hfcs is ±0.1 MHz. [b] Molecular position to which the CH_3 tensor is assigned in the spin-carrying Chl *a* (see Figure 1) of P700$^{+\bullet}$. The A_{iso} value which is indicated in Figure 7 is calculated with the equation $A_{iso} = {}^1/_3(2A_\perp + A_{||})$.

In all the mutants that were investigated, the abundance of PSI complexes in the thylakoid membrane was decreased and the optical properties of the primary donor P700 were significantly altered. In the following, the phenotype and the spectroscopic effects are discussed in relation to the type of introduced amino acid residue and with respect to the modified subunit PsaA and PsaB.

Substitution with Nonpolar Amino Acid Residues. The replacement of His(B656) and His(A676) with Leu and Phe drastically decreased the extent of stable accumulation of PSI complexes in the thylakoid membrane. Consequently, a further characterization was not possible in our hands. Similar findings were reported by Redding et al. (*21*) for Leu mutants using FUD7 as a background strain. The authors reported a decrease in the PSI activity in terms of oxygen uptake rates in thylakoid membranes of these mutants, yielding values as low as 5% of the control for HL(A676) and 10% for HL-(B656). The differences between the PSI amount reported in ref *21* and our values might be due to a generally lower PSI content in strain CC2696. The strong effect of the mutation on the accumulation of PSI is different from that of the corresponding mutations in the bRC of *Rhodobacter sphaeroides*, HL(M202) and HL(L173), in which the RC accumulates to moderate levels (*45*). The substitution with a bulky noncoordinating residue leads in these bRCs to the loss of the Mg^{2+} of the proximal BChl *a* of P_{865} and the formation of the so-called "heterodimers" consisting of one BChl and one bacteriopheophytin (BPheo) (*45*). This leads to an increased EPR line width of $P_{865}^{+\bullet}$ and to significantly larger hfcs measured by ENDOR (*45*, *60*). In the case of PSI, it was observed that the line width of the EPR signal of $P700^{+\bullet}$ is increased in the HL mutants in thylakoids (*21*). This may suggest the formation of a P700 heterodimer, but a further characterization by ENDOR spectroscopy would be required to clarify this point since the EPR line width can also be affected by several other parameters.

A possible explanation for the low PSI abundance in these mutants might be that the arrangement of the α-helices forming the reaction center unit is more rigid in PSI than in the bRC which has indeed been concluded from a comparison of both crystal structures (*46*). Furthermore, the Chl *a* molecule itself is less flexible than BChl as it contains one additional double bond in the porphyrin plane in ring B (see Figure 1). Thus, the assembly of the PSI complex might be impaired simply by the fact that the space for the incorporation of a Chl molecule is too small, when the binding pocket is occupied by a large hydrophobic amino acid side chain. A second possible explanation for the strong decrease in PSI concentration in the HL and HF mutants might be that they are more susceptible to degradation either by self-oxidation processes upon light excitation or by a higher Chl triplet yield in the antenna when the trapping time is slowed by the mutation (*47*, *48*). This would result in an increase in the level of formation of singlet oxygen. The observation that the Leu mutations only enable photosynthetic growth under anaerobic conditions may in part support this hypothesis, whereas the very slow growth rate indicates a very small amount of PSI (*21*).

Substitution with Acidic or Basic Amino Acid Residues. To study the influence of potentially charged amino acids in the vicinity of P700 on its oxidation midpoint potential and spectroscopic properties, His(B656) was replaced with the acidic amino acid Asp and the basic amino acid Arg. The amount of PSI in HR(B656) was below the detection limit. For HD(B656), the value was extremely low; a small EPR signal due to $P700^{+\bullet}$ was observed in whole cells. However, a further isolation and characterization was not possible for both mutations. The pK_a values of about 4 and 12 for Asp and Arg, respectively, suggest that these residues might be charged in the modified PSI if water from the lumenal side of the thylakoid membrane has access to these side chains. However, inside a protein the surrounding residues and, in the case of PSI, also the cofactors strongly influence the protonation and/or deprotonation reactions of the amino acid side chains. Therefore, it is not clear whether these residues are charged in these mutants.

The volume of the side chain of Asp is smaller than that of Gln or His and comparable with those of the polar residues which are tolerated at this position. From this point of view, it is hard to understand why the uncharged form should not allow the formation of the PSI complex. Hence, we believe that at least for the Asp mutation the side chain is charged in the mutated polypeptide, perhaps only during the assembly process, and, therefore, prevents the stable accumulation of PSI.

The side chain volume of Arg is 50% larger than that of His and may also be charged. Since no PSI was detected, it cannot be clarified whether the positive charge or the volume of the residue is the reason for the failure to assemble PSI.

Substitution with Uncharged Polar (Hydrophilic) Amino Acid Residues. The replacement of His with hydrophilic amino acids is moderately tolerated in terms of PSI accumulation. The residue, which is most similar in size (side chain volume) and polarity to His, namely Gln, exhibited the smallest differences in the level of PSI formation compared to WT. We assume that the carbonyl oxygen of Gln coordinates the Mg^{2+} atom of one of the Chl *a* molecules constituting P700. The other residues, Gly, Ser, Asn, and Cys, exhibited a similar decrease in the level of accumulation of PSI except for the mutation to Cys in subunit PsaA, HC-(A676), where no PSI was detected in thylakoid membranes. The reason for the stronger impact of the Cys mutation in PsaA on PSI assembly or stability remains unclear at the present time.

To study the influence of the axial ligands on the properties of the primary donor, the PSI mutants were analyzed by optical and magnetic resonance spectroscopy. This was only possible for substitutions with uncharged polar amino acid residues. For mutants containing nonpolar, acidic, or basic side chains at the positions of His(B656) and His(A676), the accumulation of PSI was insufficient for further analysis.

Effect on the Redox Properties of $P700^{+\bullet}$/P700 Caused by Mutation of the Axial Ligands. The redox potential is a measure of the energy difference between the ground state and the oxidized (positive) state of the primary donor. The free energy of both states depends on the protein environment. In particular, the charges, permanent dipoles, and polarizability of neighboring residues can affect the energy level of $P700^{+\bullet}$, whereas the neutral ground state is influenced only to a minor extent. In the bRCs, the midpoint potential of the primary donor is 150−200 mV less positive than the value for BChl in organic solvents. Plato et al. (*49*) have calculated for the bRC of *Rhodopseudomonas viridis* that the surrounding amino acid side chains stabilize the

primary donor $P_{960}^{+\bullet}$, a BChl *b* dimer. The axial His residues contribute to the stabilization by about 20%. This can be explained by the electrostatic interaction between the positive charge on the porphyrin rings in the oxidized state and the lone electron pair of the imidazole ring of the histidines. Following that explanation, the changes in the free energy of the oxidized primary donor in the mutants are mostly related to the electrostatic properties, in particular the polarizability, of the substituting amino acid side chain. These interactions depend on the distance between the coordinating ligand and the Mg. If it is assumed that this distance increases with decreasing length of the amino acid side chain, the redox potential is also affected by the size of the introduced amino acid residue. For mutations in PsaB, the increase in the midpoint potential obviously correlates with the polarizability and size of the introduced amino acid. The substitution by Gln leads only to a small increase in the midpoint potential. The side chain of this amino acid is very similar in volume and polarizability to the replaced imidazole ring. The lone pairs of the carbonyl oxygen can stabilize the positive charge of $P700^{+\bullet}$ depending on the conformation of the side chain in this PSI complex. Asn, which has the same functional group but a shorter carbon chain, is less effective due to the longer distance between the polar groups and the porphyrin plane, resulting in a larger increase in the midpoint potential. The same increase in potential is observed for the substitution with Ser, which has the polar hydroxyl group to provide axial coordination. A much stronger impact is observed if no polarizable group is introduced as is the case for the Gly substitution. This mutation leads to an increase of 100 mV. An even higher value of about 140 mV was achieved by replacement with Cys which cannot be explained by electrostatic interactions. Therefore, we assume that in the mutant HC(B656) additional structural changes have occurred due to the large volume of the sulfur which might have changed the orientation of some other amino acid residues in the proximity of P700.

Homologous mutations of the axial ligands in the bRC lead only to minor shifts of the midpoint potential of 5 mV for substitution with Gly, 16 ± 3 mV for substitution with Asn, and 21 ± 3 mV for substitution with Ser (*50*). For these mutations in the bRC, it was suggested that a water molecule fills the cavity near the respective BChl and might provide the axial ligand to the Mg^{2+} ion (*50*, *52*). In particular, the result that was obtained for the replacement with Gly favors this interpretation for the bRC. In the case of the modified PSI complexes, the axial ligation of P700 by an adventitious water molecule is not in line with the results of the redox titration for the mutations in PsaB. In addition, the buried position of P700 in the hydrophobic core of PSI makes it rather unlikely that a water molecule is trapped in this pocket. The primary donor in the bRC is positioned much closer to the periplasmatic surface, and the cavity of the protein backbone harboring the cofactors is more open to the influx of water than in PSI (*10*).

In contrast to the substitutions in PsaB, mutations HQ(A676) and HS(A676) in PsaA increase the potential of the primary donor only slightly by about 20 mV. These results show that mutations in PsaA have a smaller impact on the midpoint potential than the substitutions in PsaB. The small influence of the introduced amino acid side chain in PsaA seems to be more indirect and not dependent on the particular residue since the change in potential is the same for the replacement of His(A676) with Gln or Ser.

We conclude, therefore, that the positive charge, and the unpaired electron, is mainly localized on P_B. The effects of the mutations are explained by changes in the electrostatic environment of this dimer half. The coordination of the donor by water in the mutated PSI complexes is not very likely. The small effect on the redox potential upon changes near P_A can be explained by slight changes in the spatial or electronic structure of this chlorophyll that is coupled to P_B but does not carry any significant amount of the positive charge (see below).

Optical Characterization of $P700^{+\bullet}$/P700 and ^{3}P700/P700. The characterization of P700 by optical spectroscopy (see Figures 3−5) did not reveal strong effects on the main spectral features of P700 in the modified PSI complexes. This indicates that the substitution with uncharged polar amino acid residues does not lead to a pheophytinization of one of the two Chl molecules comprising P700. In this case, a significant shift of the main bleaching band is expected since the excitonic coupling between a Chl *a* and Pheo *a* is quite different from that of two Chl *a* molecules (*8*). Further support for this assumption comes from the zero-field splitting (ZFS) parameters $|D|$ and $|E|$ of ^{3}P700 which reflect the energy splittings between the triplet sublevels in a zero magnetic field. The ZFS parameters of ^{3}P700 of WT PSI from *C. reinhardtii* are in good agreement with values reported previously for different PSI preparations from plants (*34*, *53*). The values are very similar to those for the triplet state of monomeric Chl *a* ($|D| = 280-305 \times 10^4$ cm^{-1}, $|E| = 38-59 \times 10^4$ cm^{-1}) (*42*, *53*, *54*). This has been taken as evidence that the triplet state of P700 is mainly localized on one half of the Chl dimer. On the basis of recent FTIR measurements, it has been also proposed that the ^{3}P700/P700 difference spectra originate from a single Chl *a* molecule (*17*).

In the mutants, the ZFS parameters were only changed to a minor extent (see Table 3), suggesting that the distribution of the triplet state is not significantly altered and that the triplet state remains on a single Chl *a* molecule. The unchanged T − S spectrum in the wavelength regions between 450 and 650 nm and between 700 and 850 nm, representing mainly the triplet absorption, supports this interpretation (not shown). It should be noted that $|D|$ and $|E|$ values for Chl *a* in vitro are solvent-dependent, and changes by as much as 10% have been observed and related to the variation of the axial ligand(s) to the central Mg^{2+} of Chl *a* (*42*). This is in full accordance with our experiments on PSI and underlines the conclusion that the mutations are not influencing the triplet state in a significant way.

The interpretation of the changes observed in the optical measurements of mutated PSI complexes is discussed in more detail below. The different contributions to the T − S spectrum have been analyzed for PSI preparations from plants (*34*, *51*, *53*). (i) Upon triplet formation, both excitonic absorption bands of P700 (a dimer composed of two excitonically coupled Chl molecules) are bleached. The main bleaching band at 695 nm has been assigned to the disappearance of the low-energy excitonic band. It accounts for the majority of the oscillator strength of P700 in the Q_y-region. The position of the high-energy exciton band is a controversial topic in the literature (*51*). (ii) Upon triplet

formation, the excitonic interaction is lost, resulting in two noninteracting Chls, one in the triplet state and one in the singlet ground state. This gives rise to the appearance of an absorption band with half the oscillator strength of the dimer attributed to the Q_y transition of the Chl *a* which is not carrying the triplet state. Measurements using linear dichroic ADMR favor weak positive bands at 692 nm or at 682 nm in spinach PSI as candidates for this monomer absorption (*51*). The absorption of the Chl triplet state is weak and broad between 600 and 800 nm (*66*). (iii) Changes in the absorption bands of neighboring Chls [e.g., accessory Chls and the primary acceptor(s)] are observed in the T − S spectrum because P700 in the triplet state has a different excitonic interaction with Chls in its proximity than in the singlet state. Spectral features in the wavelength region between 650 and 680 nm are attributed to these changes in coupling (*51*). If the triplet state is localized on only one Chl, it is mainly the interaction between this Chl *a* of the dimer and the accessory Chls or the primary acceptor(s) that is changed upon triplet formation. The Chl *a* which is not carrying the triplet is still in its singlet ground state after triplet formation of P700. Therefore, only minor changes in the interaction between the other half of the dimer and neighboring Chls are expected upon triplet formation.

The T − S spectrum of PSI from WT *C. reinhardtii* resembles the features reported for different PSI preparations from spinach, except for the fact that the main bleaching band is shifted by about 5 nm to 694.5 nm and that the feature around 682 nm, recently measured in PSI from spinach (*34*), is missing in PSI preparations and thylakoids from the green algae. This difference with respect to higher plants might be caused by variations in the amino acid sequence in *C. reinhardtii*. Despite the fact that the amino acid sequences in higher plants and green algae are more than 80% identical (*4*, *5*), the molecular surroundings of the primary donors are slightly different.

Compared to that of WT (see Figure 5, solid line), the T − S spectra of the PSI mutants showed two main effects. (i) The main bleaching band is slightly blue shifted and narrower for PsaA and PsaB mutants. Since the position of the main bleaching band is related to the strength of the excitonic coupling between the two Chls of the dimer, a blue shift indicates that this interaction is affected by the mutation. Obviously, the excitonic coupling between the two Chls is changed in PsaA and PsaB mutants to the same extent. (ii) Changes in the spectral features between 650 and 680 nm were only observed when the mutation was introduced into subunit PsaB. If the substituted ligand influences the interactions between P_B and nearby pigments (e.g., the accessory Chls), it becomes primarily visible in the T − S spectrum for the Chl *a* carrying the triplet state. Consequently, our observations that only mutations in PsaB significantly alter the spectral features in the wavelength region between 650 and 680 nm lead us to the conclusion that the triplet state is localized on P_B.

The changes in the absorption difference spectra of $P700^{+\bullet}$/P700 at low temperatures (Figure 3) are in accordance with the analysis of the T − S measurements: blue shift and narrowing of the main bleaching band and in addition, for mutations in PsaB, distortions in the 650−680 nm region. The absorption difference spectrum of $P700^{+\bullet}$/P700 at low temperatures of PSI complexes from WT is interpreted in a similar way as described above for the T − S spectrum (*67*). In addition to the latter measurement, the absorbance difference spectrum contains a strong electrochromic band shift of a Chl absorbing around 688 nm in response to the formation of $P700^{+\bullet}$. In fact, addition of one S-shaped line, representing the electrochromic bandshift, to the T − S spectrum centered around 688 nm, yields good agreement with the $P700^{+\bullet}$/P700 spectrum (not shown). Spectral features in the wavelength region between 650 and 680 nm are attributed to changes in the interaction between P700 and neighboring Chls upon $P700^{+\bullet}$ formation similar to the interpretation of the T − S measurement.

The observation that only mutations of His(B656) in PsaB affect these features supports our assumption made from the results of the midpoint potential measurements that in the $P700^{+\bullet}$ state the unpaired electron spin is localized on P_B. In contrast to the T − S data, the low-temperature absorption spectra for all PsaB mutants, except HQ(B656), have a very similar line shape more or less independent of the amino acid residue that replaces the histidine. Probably, the strong bathochromic effect of the positive charge in the oxidized state covers the influence of the substituted amino acid side chain on the absorbance difference spectrum.

The localization of both, the unpaired electron and the triplet state, on P_B contradicts a recent interpretation of FTIR studies on the primary donor of P700 (*17*). Breton et al. assigned shifts in the carbonyl region to 13^1-keto and the 13^2-ester carbonyl modes to each of the two Chls comprising P700 and suggested that the Chl *a* harboring the triplet state is not carrying the major part of the electron hole in the oxidized state (*17*). It is, however, not fully understood how the formation of the triplet state or an unpaired electron is influencing the vibrational modes on substituents of the porphyrin ring. The assigned 13^1-keto and the 13^2-ester modes can also have a dipolar interaction with the second Chl *a* which is in proximity. This kind of influence is, of course, highly dependent on the orientation of the substituents in the binding pocket of P700. The change in vibrational absorbance is, therefore, not a direct measure for the localization of the triplet state or an electron spin as long as the structure of P700 and its surroundings are not resolved to atomic resolution.

The oxidized-minus-reduced spectrum of $P700^{+\bullet}$/P700 at room temperature exhibits an additional bleaching band at 665 nm for mutations in PsaB, whereas the substitution of His(A676) in PsaA leads to an absorbance decrease around 685 nm. The very pronounced effect observed for HG(B656), HC(B656), HS(B656), and HN(B656) in the room-temperature absorbance difference spectra is less visible at low temperatures due to the superimposed electrochromic band shifts of neighboring Chl *a* molecules whose amplitudes increase strongly with decreasing temperature (not shown). The nature of the introduced amino acid side chain influences this feature only to a minor extent. The origin of the additional bleaching band at 665 nm is still unclear. The most plausible explanation is an altered excitonic interaction between the two Chls of P700 (see also ref *20* for a more detailed discussion).

Distribution of the Electron Spin in $P700^{+\bullet}$. At first glance, it is quite surprising that the substitution of one of the axial ligands of P700 is only introducing small effects on the electron spin distribution of the oxidized primary donor when

His(B656) is substituted and that no change is observed when His(A676) is replaced with other amino acid residues. However, the spin density on the Mg^{2+} which is coordinated by the axial ligand is probably quite small as ^{25}Mg ENDOR measurements performed on BChl $a^{+\bullet}$ revealed (*61*). This finding is also supported by the fact that the exchange of the central metal atom to Zn^{2+} has only minor effects on the spin distribution of the BChl *a* and Chl *a* cation radical in solution (*59*). The observed increase of a single hfc of $P700^{+\bullet}$ in the mutated PSI complexes is also not expected for the exchange of an axial ligand. Instead, the introduced amino acid side chain should more or less influence the hfcs in a similar manner at least for the well-resolved proton hfcs of the methyl groups because it is most likely positioned above the chlorin plane. The exclusive increase of the ^1H hfc for the methyl group at position 12 rather indicates a modification in the local environment of this methyl group. To explain the distortions of the hfcs found for the substitution of His(B656), we propose that the introduced residue in PsaB affects the position of the Mg^{2+} in the porphyrin plane of P_B to some extent. Especially, the replacements by amino acid side chains shorter than that of His might result in a small displacement of the metal ion if it is no longer well-coordinated. The loss of one of the fixing points of P_B in the protein scaffold might then result in a conformational change of the chlorin ring of this Chl *a*. The optical difference spectra of the mutants (see above) support this interpretation as the blue shifts of the main bleaching band indicate a change in the distance or orientation of P_A and P_B relative to each other. Additional evidence for this assumption comes from the small increase in the hfc at position 12 for the substitution with Gln which provides a similar ligation as His, whereas the other substitutions of His(B656) have a stronger impact on this hfc (Table 3 and Figure 6). Interestingly, the latter cases show almost the same results in the ENDOR measurements, although the sizes of the amino acid side chains differ substantially (Asn → Gly). We suppose that the replacement of His with Gln still allows a ligation of the Mg^{2+} of P_B, but the amino acid side chains of Asn, Ser, Gly, and Cys do not or only weakly coordinate the central metal ion of this Chl *a*. Without the (strong) axial ligation, P_B can adopt a different conformation determined by the remaining binding partners. In this model, the influence of the introduced amino acid side chain, which is not ligating the Mg^{2+} of P_B, is then small. The results from optical spectroscopy support the minor interaction of the particular residue with P_B because the difference spectra for the substitution of His(B656) are very similar except for the replacement with Gln (Figures 2−5). The increase in the ^1H hfc of the methyl group at position 12 is then caused by a movement of P_B or a change in its conformation. This methyl group positioned on ring C of the chlorin macrocyle is in proximity to exocyclic ring E. EPR and ENDOR studies on BChl *a* and Chl *a* have shown that the hfc of the methyl group at position 12 is very sensitive to modifications of the neighboring ring E (*57*−*59*). In PSI, the keto oxygen at molecular position 13^1 or the oxygen of the methyl ester group at position 13^2 of Chl *a* (Figure 1) might interact with the environment, e.g., with nearby amino acid side chains or with the second Chl as suggested above. A small displacement of P_B caused by the substitution of His(B656) with a nonligating residue might influence the interaction of the protein backbone and ring E, leading to a conformation different from WT. From this point of view, the change in the ^1H hfc of the methyl group at ring C indicates an interaction of P_B with the protein framework of the Chl *a* molecule. The change in the ^1H hfc of the β-protons at positions 17^1 and 18^1 of P_B is also interpreted as resulting from a slight conformational change in the spin-carrying Chl *a* (Figure 6).

Interestingly, the substitutions of His(A676) in PsaA show no influence on the spin distribution in the ENDOR spectra. These results corroborate the assignment of the ^1H hfcs of the methyl groups and of the β-protons 17^1 and 18^1 to P_B, exclusively, and confirm the interpretation of the optical results. In other words, the spin density of $P700^{+\bullet}$ is mainly localized on the Chl *a* axially coordinated by PsaB. Käss et al. suggested that the linepairs 1′, 1 and 2′, 2 might contain contributions of the methyl protons from the other Chl half of P700 (*39*, *44*, *56*) which is P_A according to our assignment. If the replacement of His(A676) is also inducing a slight displacement of P_A, it is expected to influence these small hfcs. The magnitude of this effect is, however, dependent on the interaction of P_A with its environment and it is therefore possible that no significant changes for the small hfcs of this molecule might be seen. Since the surroundings of the two Chls are not yet known to atomic resolution, it is not possible to determine with certainty whether the unpaired electron is exclusively localized on P_B. However, all analyzed properties of P700 in the mutated PSI complexes strongly support the fact that both the unpaired electron and the triplet state are at least very asymmetrically shared between the two halves of the dimer and are mainly localized on P_B that is axially coordinated by His(B656).

CONCLUSIONS

Our work shows that quite a few amino acid residues can substitute one of the axial ligands of P700 without striking effects on the biophysical properties. We assume that for the cases where no or only low levels of the PSI complex were accumulated the assembly and not the function of the photosystem was impaired. The comparison of the biophysical properties for analogous mutations in PsaA and PsaB shows that the unpaired electron of $P700^{+\bullet}$ and the triplet state are mainly localized on the P_B chlorophyll of P700. This is the Chl *a* of the excitonically coupled dimer bound to helix m′ and called eC_1' in the 4 Å structural model (*10*, *11*). It still remains unclear how the protein environment adjusts the special properties of the Chl *a* dimer. In particular, the very low midpoint potential of the primary electron donor remains quite an enigma. However, our experiments have shown that the surrounding amino acid side chains play a significant role in the fine-tuning of such properties of P700. For a further understanding of the light-induced charge separation, a high-resolution structure of PSI is required to identify other interaction sites of the dimer with the protein scaffold which can be used as probes for additional mutagenesis studies.

ACKNOWLEDGMENT

We thank Uwe Fink for the preparation of PSI complexes and Marianne Çetin (both Technische Universität Berlin) for excellent technical assistance. Many helpful discussions with

Friedhelm Lendzian (Technische Universität Berlin) are gratefully acknowledged.

REFERENCES

1. Golbeck, J. H. (1992) *Annu. Rev. Plant Physiol. Plant Mol. Biol. 43*, 293−324.
2. Chitnis, P. R. (1996) *Plant Physiol. 111*, 661−669.
3. Brettel, K. (1997) *Biochim. Biophys. Acta 1318*, 322−373.
4. Fish, L. E., K¸ck, U., and Bogorad, L. (1985) in *Molecular Biology of the Photosynthetic Apparatus*, pp 111−120, Cold Spring Harbor Laboratory Press, Plainview, NY.
5. Vallon, O. M., and Bogorad, L. (1993) *Eur. J. Biochem. 214*, 907−915.
6. Stowell, M. H., McPhillips, T. M., Rees, D. C., Soltis, S. M., Abresch, E., and Feher, G. (1997) *Science 276*, 812−816.
7. Huber, M. (1997) *Photosynth. Res. 52*, 1−26.
8. Allen, J. P., and Williams, J. C. (1995) *J. Bioenerg. Biomembr. 27*, 275−283.
9. Artz, K., Williams, J. C., Allen, J. P., Lendzian, F., Rautter, J., and Lubitz, W. (1997) *Proc. Natl. Acad. Sci. U.S.A. 94*, 13582−13587.
10. Schubert, W.-D., Klukas, O., Krauss, N., Saenger, W., Fromme, P., and Witt, H. T. (1997) *J. Mol. Biol. 272*, 741−769.
11. P., Fromme, P., Witt, H. T., and Saenger, W. (1998) in *Photosynthesis: Mechanism and Effects* (Garab, G., Ed.) Vol. 1, pp 603−606, Kluwer, Dordrecht, The Netherlands.
12. Davis, I. H., Heathcote, P., MacLachlan, D. J., and Evans, M. C. W. (1993) *Biochim. Biophys. Acta 1143*, 183−189.
13. Rigby, S. E. J., Nugent, J. H. A., and O'Malley, P. J. (1994) *Biochemistry 33*, 10043−10050.
14. Käss, H., and Lubitz, W. (1996) *Chem. Phys. Lett. 251*, 193−203.
15. Käss, H., Frome, P., and Lubitz, W. (1996) *Chem. Phys. Lett. 257*, 197−206.
16. Mac, M., Bowlby, N. R., Babcock, G. T., and McCracken, J. (1998) *J. Am. Soc. 120*, 13215−13223.
17. Breton, J., Nabedryk, E., and Leibl, W. (1999) *Biochemistry 38*, 11585−11592.
18. Cui, L., Bingham, S. E., Kuhn, M., Käss, H., Lubitz, W., and Webber, A. N. (1995) *Biochemistry 34*, 1549−1558.
19. Krabben, L., Käss, H., Schlodder, E., Kuhn, M., Lubitz, W., Xu, H., Bingham, S. E., and Webber, A. N. (1995) in *Photosynthesis: from light to biosphere* (Mathis, P., Ed.) Vol. 2, pp 123−126, Kluwer, Dordrecht, The Netherlands.
20. Webber, A. N., Su, H., Bingham, S. E., Käss, H., Krabben, L., Kuhn, M., Jordan, R., Schlodder, E., and Lubitz, W. (1996) *Biochemistry 35*, 12857−12863.
21. Redding, K., MacMillan, F., Leibl, W., Brettel, K., Hahnley, J., Rutherford, A. W., Breton, J., and Rochaix, J.-D. (1998) *EMBO J. 17*, 50−60.
22. Amesz, J., and Hoff, A. J. (1996) *Biophysical Techniques in Photosynthesis*, Kluwer, Dordrecht, The Netherlands.
23. Lee, H., Bingham, S. E., and Webber, A. N. (1998) *Methods Enzymol. 297* (in press).
24. Boyton, J. E., Gillham, N. W., Harris, E. H., Hosler, J. P., Johnson, A. M., Jones, A. R., Randolph-Anderson, B. L., Robertson, D., Klein, T. M., Skark, K. B., and Sanford, J. C. (1988) *Science 240*, 1534−1538.
25. Webber, A. N., Gibbs, P. B., Ward, J. B., and Bingham, S. E. (1993) *J. Biol. Chem. 268*, 12990−12995.
26. Owens, T. G., Webb, S. P., Mets, L., Alberte, R. S., and Felming, G. R. (1989) *Biophys. J. 56* (1), 95−106.
27. Harris, E. H., Ed. (1989) *Chlamydomonas Sourcebook*, Academic Press, San Diego.
28. Gerken, S., Dekker, J. P., Schlodder, E., and Witt, H. T. (1989) *Biochim. Biophys. Acta 977*, 52−61.
29. Hiyama, T., and Ke, B. (1972) *Biochim. Biophys. Acta 267*, 160−171.
30. Rautter, J., Lendzian, F., Wang, S., Allen, J. P., and Lubitz, W. (1994) *Biochemistry 33*, 12077−12084.
31. Zweygart, W., Thanner, R., and Lubitz, W. (1994) *J. Magn. Reson. 109*, 172−177.
32. Crystall, B., Booth, P. Y., Klug, D. R., Barber, J., and Porter, G. (1989) *FEBS Lett. 269*, 138−140.
33. Setif, P., and Bottin, P. (1989) *Biochemistry 28*, 2689−2697.
34. Carbonera, D., Collareta, P., and Giacometti, G. (1997) *Biochim. Biophys. Acta 1322*, 115−128.
35. Carbonera, D., Giacometti, G., and Agostini, G. (1994) *FEBS Lett. 343*, 200−204.
36. HD and HR were expressed in FUD7 which is defective in PSII expression.
37. Mullet, J. E., Burke, J. J., and Arntzen, C. J. (1980) *Plant Physiol. 65*, 814−822.
38. Krabben, L. (1999) Ph.D. Thesis, Technische Universität Berlin, Berlin.
39. Käss, H. (1995) Ph.D. Thesis, Technische Universität Berlin, Berlin.
40. Watanabe, T., and Kobayashi, M. (1991) in *Chlorophylls* (Scheer, H., Ed.) pp 287−303, CRC Press, Boca Raton, FL.
41. Hoff, A. J. (1996) in *Biophysical Techniques in Photosynthesis* (Amesz, J., and Hoff, A. J., Eds.) pp 277−298, Kluwer, Dordrecht, The Netherlands.
42. Angerhofer, A. (1991) in *Chlorophylls* (Scheer, H., Ed.) pp 945−991, CRC Press, Boca Raton, FL.
43. Lubitz, W., and Lendzian, F. (1996) in *Biophysical Techniques in Photosynthesis* (Amesz, J., and Hoff, A. J., Eds.) pp 255−275, Kluwer, Dordrecht, The Netherlands.
44. Käss, H., Fromme, P., Witt, H. T., and Lubitz, W. (2000) *J. Phys. Chem. B* (submitted).
45. Huber, M., Lous, E. J., Isaacson, R. A., Feher, G., Gaul, D., and Schenck, C. C. (1990) in *Reaction Centers of Photosynthetic Bacteria* (Michel-Beyerle, M. E., Ed.) pp 219−228, Springer-Verlag, Berlin; *Proc. Natl. Acad. Sci. U.S.A. 85*, 7226−7230.
46. Schubert, W.-D., Klukas, O., Saenger, W., Witt, H. T., Fromme, P., and Krauss, N. (1998) *J. Mol. Biol. 280*, 297−314.
47. Spreitzer, R. J., and Metz, L. (1981) *Plant Physiol. 647*, 565−569.
48. Setif, P. (1992) in *The Photosystems: Structure, Function and Molecular Biology* (Barber, J., Ed.) pp 471−499, Elsevier, New York.
49. Plato, M., Lubitz, W., Lendzian, F., and Möbius, K. (1988) *Isr. J. Chem. 28*, 109−119.
50. Schulz, C., Müh, F., Beyer, A., Jordan, R., Schlodder, E., and Lubitz, W. (1998) in *Photosynthesis: Mechanisms and Effects* (Garab, G., Ed.) Vol. 2, pp 767−770, Kluwer, Dordrecht, The Netherlands.
51. Vrieze, J., Gast, A. J., and Hoff, A. J. (1996) *J. Phys. Chem. 100*, 9960−9967.
52. Goldsmith, J. O., King, B., and Boxer, S. G. (1996) *Biochemistry 35*, 2421−2428.
53. Den Blanken, H. J., and Hoff, A. J. (1983) *Biochim. Biophys. Acta 724*, 52−61.
54. Rutherford, A. W., and Mullet, J. E. (1981) *Biochim. Biophys. Acta 635*, 225−235.
55. Siekmann, I., Brettel, K., Bock, C., Van der Est, A., and Stehlik, D. (1993) *Biochemistry 32*, 4842−4847.
56. Käss, H., Bittersmann-Weidlich, E., Andreasson, L.-E., Bönigk, B., and Lubitz, W. (1995) *Chem. Phys. 194*, 419−432.
57. Scheer, H., Katz, J. J., and Norris, J. R. (1977) *J. Am. Chem. Soc. 99*, 1372−1377.
58. Käss, H., Rautter, A., Zweygart, W., Struck, A., Scheer, H., and Lubitz, W. (1994) *J. Phys. Chem. 98* (1), 354−364.
59. Käss, H., Lubitz, W., Hartwig, G., Scheer, H., Noy, D., and Scherz, A. (1998) *Spectrochim. Acta A54*, 1141−1156.
60. Rautter, J., Lendzian, F., Schulz, C., Fetsch, A., Kuhn, M., Lin, X., Williams, J. C., Allen, J. P., and Lubitz, W. (1995) *Biochemistry 34*, 8130−8143.
61. Lendzian, F., Möbius, K., Plato, M., Smith, U. H., Thurnauer, M. C., and Lubitz, W. (1984) *Chem. Phys. Lett. 111*, 583−588.
62. Kühlbrandt, W., and Wang, D. N. (1991) *Nature 350*, 130−134.

63. Trocha, M. (1997) Diplomarbeit, Technische Universität Berlin, Berlin.
64. Beyer, A. (1998) Diplomarbeit, Technische Universität Berlin, Berlin.
65. Bylina, E. J., Kolaczkowski, S. V., Norris, J. R., and Youvan, D. C. (1990) *Biochemistry 29*, 6203−6210.
66. Linschitz, H., and Sarkanen, K. (1958) *J. Am. Chem. Soc. 80*, 4826−4832.
67. Schaffernicht, H., and Junge, W. (1982) *Photochem. Photobiol. 39*, 407−417.
68. Cantor, C., and Schimmel, P. R. (1980) in *Biophysical Chemistry Part II: Techniques for the Study of Biological Structure and Function*, pp 349−408, W. H. Freeman, San Francisco.

BI001200Q